JOURNAL OF MATERIALS SCIENCE 30 (1995) 212–218

The effect of particles on the critical strain associated with the Portevin–LeChatelier effect in aluminium alloys

K. S. CHAN, L. H. CHEN, T. S. LUI
National Cheng-Kung University, Department of Materials Science and Engineering, Tainan, 70101 Taiwan

The effect of particles on the critical strain, ε_c, associated with the Portevin–LeChatelier (PL) effect of aluminium alloys is studied using Al–Mg–Ni and Al–Si alloys. Al–Mg–Ni and Al–Si alloy matrixes are composed of Al_3Ni and Si particles, respectively. Tensile tests were performed in the temperature range 223–273 K in which the critical strain decreases with increasing temperature, and strain rates between 10^{-5} and $10^{-2}\ s^{-1}$ were chosen. According to the apparent activation energies, Q, Mg and Si solute atoms are responsible for the flow instability in Al–Mg–Ni and Al–Si alloys, respectively. The experimental results also show that the critical strain decreases with decreasing particle spacing, d_p. Since the particle spacing is small compared to the corresponding grain size, the decrease in critical strain should be ascribed to the effect of particles. Considering that the dislocation density is increased by the particles, a modified model showing the critical strain, ε_c, as a function of particle spacing, d_p, is proposed as $\dot{\varepsilon} \propto \varepsilon_c^{\beta(\gamma+1/2)} d_p^{-n(\gamma+1/2)} T^{-1} \exp(-Q/kT)$, in which $\dot{\varepsilon}$, T and k are the strain rate, temperature and Boltzmann constant, respectively. Linear fit of the plots of ln ε_c versus ln d_p and ln $\dot{\varepsilon}$ versus ln d_p indicates that this equation is appropriate to rationalize the particle effect on the critical strain.

1. Introduction

Aluminium alloys often exhibit serrated flow after a critical strain, ε_c, during tensile deformation in the temperature range 223–373 K. This phenomenon is attributed to the Portevin–LeChatelier (PL) effect [1, 2]. Associated with the PL effect, the alloys will be strengthened, have lower ductility and surface marking may be induced during cold working, etc.; so that many studies on the PL effect have been performed. However, most studies have concentrated on single phase alloys, such as Al–Mg and solution treated Al–Mg–Si alloy [3–7], etc. Recently, particles are often applied to strengthen the alloys at both low and high temperature. Since both the mechanical properties and processing of these aluminium alloys in the temperature range 223–373 K are affected by the PL effect, studies concerning the effect of particles on the PL effect in aluminium alloys with particles are necessary. Since the rigid particles can affect the motion of dislocation [8, 9], the effect of particles on the PL effect is assumed.

As Ni is nearly insoluble in the α matrix [10] and forms hard Al_3Ni particles during solidification [11], Ni is used to strengthen the aluminium alloys. Also, Ni has no reaction with Mg solute, so that the Al–Mg–Ni alloys can be considered as Al–Mg alloys with the addition of Al_3Ni particles. In Al–Si alloys, the matrix microstructure consists of Si particles, when the Si content is approximately greater than 1 wt % [12]. As a result, both of these aluminium alloys contain a distribution of particles in the matrix. Then, the effect of particles on the PL effect is studied using Al–Mg–Ni and Al–Si alloys in which Mg [3, 13] and Si [14] in the matrix are responsible for the flow instability, respectively.

The critical strain shows two kinds of temperature dependence. Al–Mg [3, 6] and Al–Si [14] alloys are two typical examples for each kind of temperature dependence. In Al–Mg alloys, the critical strain decreases to a minimum initially, and then increases with increasing temperature [3]. The critical strain in Al–Si alloys decreases monotonously to a minimum with increasing temperature, and is maintained at minimum afterwards [14]. Regardless of the different behaviour at high temperature, both alloys have critical strain decreasing with increasing temperature below room temperature. In this low temperature regime, critical strain ε_c, can be expressed as a function of strain rate, $\dot{\varepsilon}$, temperature, T, such that

$$\dot{\varepsilon} \propto \varepsilon_c^{\alpha} \exp(-Q/kT) \quad (1)$$

where the exponent α correlates the critical strain to vacancy concentration and dislocation density [3, 13, 15], Q and k are the apparent activation energies and Boltzmann constant, respectively. Accordingly, tensile tests are performed on the Al–Mg–Ni and Al–Si alloys in the temperature range 223–273 K, in which the critical strain decreases with increasing

0022–2461

temperature. The effect of particles on the critical strain is emphasized.

Recently, Chen *et al.* [16–18] have proposed a modified model adopting the concept of average dislocation velocity from McCormick [19] and local vacancy enrichment near the dislocation core [16–18] to rationalize the α in Equation 1. In the present study, a model is put forward by considering the relation between dislocation density and particle spacing, and is used to account the effect of particles.

2. Modified model

In this section, the model proposed by Chen *et al.* [16–18], is introduced. Furthermore, the dislocation density as a function of grain size is considered, so that an expression of critical strain as a function of grain size is obtained.

The Orowan equation states that

$$\dot{\varepsilon} \propto \rho_m b V \tag{2}$$

where $\dot{\varepsilon}$, ρ_m, b and V are the tensile strain rate, mobile dislocation density, Burgers vector and average dislocation velocity, respectively. With L as the average pinning distance of a mobile dislocation McCormick [19] has taken the average dislocation velocity, V, as

$$V = L/t_a \tag{3}$$

where t_a is the total ageing time, including the time of motion and the static ageing time while the dislocation is momentarily arrested. McCormick has assumed that the onset of flow instability occurs when t_a is equal to that required for permanent dislocation locking, and t_a can be written in terms of diffusivity, D, and temperature, T, as

$$t_a \propto T/D \tag{4}$$

and D is expressed as

$$D \propto C_v \exp(-Q/kT) \tag{5}$$

where C_v, Q and k are the vacancy concentration, activation energy and Boltzmann constant, respectively. Combining Equations 2–5, one obtains

$$\dot{\varepsilon} \propto \rho_m C_v L T^{-1} \exp(-Q/kT) \tag{6}$$

According to Mukherjee *et al.* [20], the average dislocation pinning distance, L, can be interpreted in terms of ρ_m as

$$L = \rho_m^{-1/2} \tag{7}$$

Chen *et al.* [16–18] have shown that the vacancy concentration should be more properly expressed in terms of mobile dislocation density using the concept of local dislocation enrichment near the dislocation core region of the mobile dislocation, such that

$$C_v \propto \rho_m^{\gamma} \tag{8}$$

Substituting Equations 7 and 8 into Equation 6, one obtains

$$\dot{\varepsilon} \propto \rho_m^{(\gamma+1/2)} T^{-1} \exp(-Q/kT) \tag{9}$$

For single phase alloys, the dislocation density can be correlated with strain according to [21, 22]

$$\rho_m \propto \varepsilon^{\beta} \tag{10}$$

so that

$$\dot{\varepsilon} \propto \varepsilon_c^{\beta(\gamma+1/2)} T^{-1} \exp(-Q/kT) \tag{11}$$

The less sensitive term T^{-1} is often dropped for empirical fit, and the temperature dependence is approximated by $\exp(-Q/kT)$ [13–18, 22]. Hence, the exponent α in Equation 1 is equal to $\beta(\gamma + 1/2)$. By considering the grain size effect, Charnock [23, 24] proposed that the dislocation density should be a function of grain size, d_g, as

$$\rho_m \propto \varepsilon^{\beta} d_g^{-n_g} \tag{12}$$

and then

$$\dot{\varepsilon} \propto \varepsilon_c^{\beta(\gamma+1/2)} d_g^{-n_g-(\gamma+1/2)} T^{-1} \exp(-Q/kT) \tag{13}$$

Chen *et al.* have shown that the grain size dependence of the critical strain can be more properly expressed by Equation 13.

In the present investigation, Equations 12 and 13 are modified, and are used to illustrate the effect of particles on the critical strain of Al–Mg–Ni and Al–Si alloys within the low temperature regime in which the critical strain decreases with temperature.

3. Experimental procedure

The Ni content in the Al–Mg–Ni alloys was varied from 0.5 to 6 wt % within the hypoeutectic composition. The Mg content was kept at about 2.7 wt %, as a higher Mg content may lead to the precipitation of Al_3Mg_2. Al–Si alloys having Si contents of 1, 4, 7 and 11 wt % were used. The composition was all chosen within the hypoeutectic composition, because the hypereutectic composition will give an uneven distribution of particles within the matrix. The alloys were prepared from pure aluminium (99.7 wt %), master alloys of Al–10 Mg, Al–10 Ni and Al–10 Si (in wt %). The alloys were melted in an induction furnace and billets with 72 mm diameter and 200 mm length were cast. The chemical compositions of the Al–Mg–Ni and Al–Si alloys, determined via emission spectroscopy, are given in Table I and II, respectively. After being solution treated at 773 K for 24 h, the billets were extruded as rods of 14 mm diameter. Then, tensile specimens, with gauge sections 6 mm in diameter and 35 mm in length, were machined.

Before the tensile test, tensile specimens of Al–Mg–Ni and Al–Si alloys were annealed at 773 K for 1.5 h and 10 h, respectively. Tensile tests were performed by an Instron type machine in the temperature range 223–273 K. The temperatures were achieved by a bath of ethanol and solid carbon dioxide. Strain rates were selected in the range 10^{-5} to 10^{-2} s^{-1}. At least three tensile specimens were tested for each condition.

The microstructures of the alloys were examined by an optical microscope and the phases were confirmed by X-ray diffraction. Polarized light was used to observe the grain size of Al–Mg–Ni alloys. Particle spacing were measured by an image analyser and each datum is an average of 100 measurements.

TABLE I Chemical composition of the Al–Mg–Ni alloys

Alloy	Ni	Mg	Si	Cu	Zn	Fe	Mn	Al
Al–Mg (wt %)	0.04	2.63	0.04	0.002	0.003	0.16	0.01	Balance
0.5 Ni (wt %)	0.46	2.59	0.06	0.003	0.005	0.14	0.01	Balance
1.0	0.86	2.67	0.04	0.002	0.004	0.15	0.01	Balance
2.0	1.76	2.73	0.04	0.002	0.005	0.13	0.01	Balance
3.0	2.83	2.67	0.04	0.002	0.006	0.13	0.01	Balance
4.0	3.81	2.89	0.04	0.002	0.005	0.14	0.01	Balance
5.0	5.05	2.95	0.04	0.003	0.008	0.14	0.02	Balance
6.0	6.29	2.95	0.04	0.002	0.008	0.13	0.02	Balance

TABLE II Chemical composition of the Al–Si alloys

Alloy (wt % Si)	Si	Mg	Fe	Cu	Al
1	1.0	0.020	0.14	0.045	Balance
4	3.9	0.013	0.17	0.030	Balance
7	6.7	0.013	0.14	0.001	Balance
11	11.3	0.011	0.18	0.030	Balance

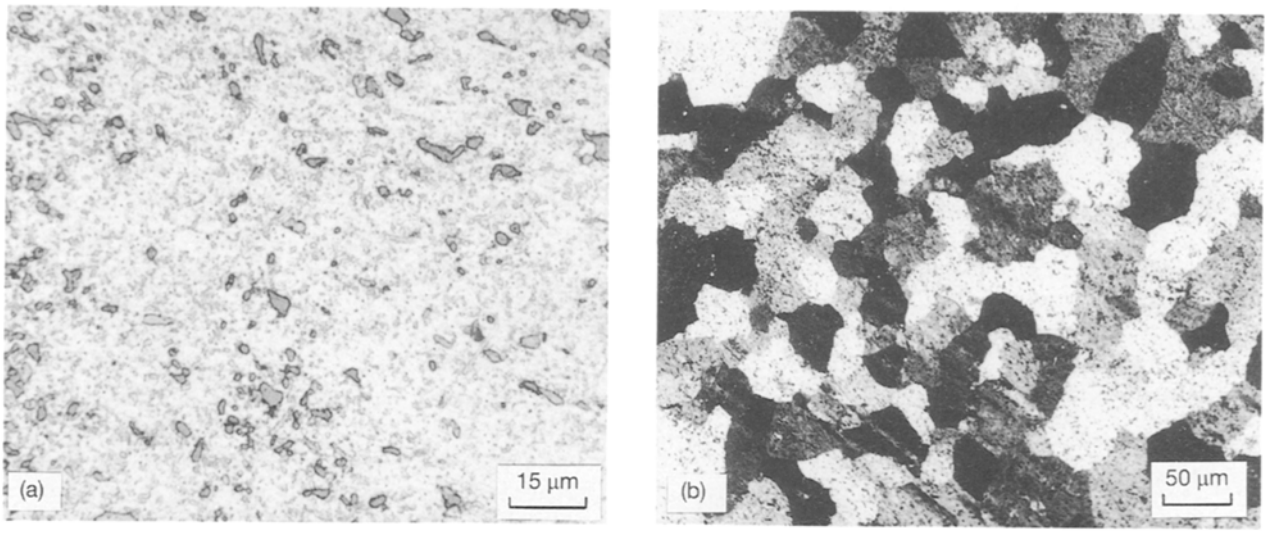

Figure 1 Microstructure of the 4 wt % Ni alloys showing: (a) the distribution of particles, and (b) grain size, after extrusion and solution treatment.

4. Results and discussion

4.1. Microstructure

The microstructure of the Al–Mg–Ni and Al–Si alloys is shown in Figs 1 and 2, respectively. The particles are Al_3Ni in Al–Mg–Ni alloys, while Si particles are obtained in Al–Si alloys. The particle size is about 1–5 μm. With the increase of alloy content, the volume fraction of the particles increases, and the particle spacing decreases strictly. Quantitative measurements of particle spacing, d_p, volume fraction, V_f, and grain size, d_g, are given in Tables III and IV. The grain size is about 35–50 μm, except for the alloy with 5 wt %Ni, having size about 13 μm. On the other hand, particle spacing decreases strictly from 36 to 12 μm with Ni content. In Al–Si alloys, particle spacing varies from 190 to 45 μm, which is less than the corresponding grain size. According to the observation of microstructure, particle spacing should have a dominant effect compared to the grain size.

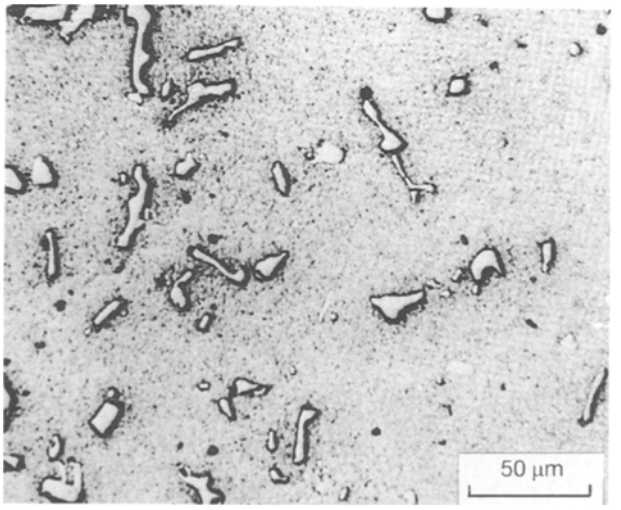

Figure 2 Microstructure of the 7 wt % Si alloy after extrusion and solution treatment.

TABLE III Quantitative measurement of the Al–Mg–Ni alloy microstructure

Alloy (wt % Ni)	V_f (%)	d_g (μm)	d_p (μm)
0.5	0.84	50	36.00
1.0	1.88	45	32.36
2.0	2.06	36	25.34
3.0	3.74	35	18.87
4.0	4.22	35	16.18
5.0	4.88	13	12.12
6.0	7.35	36	12.95

TABLE IV Quantitative measurement of the Al–Si alloy microstructure

Alloy (wt % Si)	V_f (%)	d_g (μm)	d_p (μm)
1	1.0	240	190
4	4.3	200	75
7	9.6	170	63
11	14.6	120	45

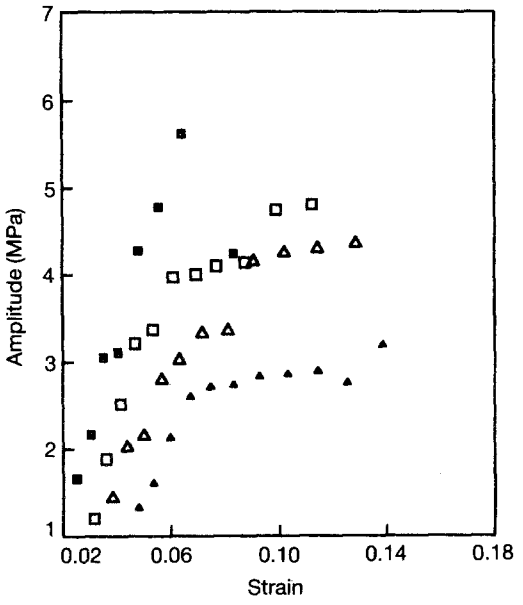

Figure 3 The amplitude of the serration on the flow curves of Al–Mg–Ni alloys at 248 K and $5.7 \times 10^{-4}\ s^{-1}$ as a function of strain: (▲) Al–Mg, (△) 0.5 wt % Ni, (□) 1 wt % Ni, (■) 4 wt % Ni.

4.2. General features

Within the strain rates 10^{-5} to $10^{-2}\ s^{-1}$, both alloys exhibit A type serration and critical strain decreases with increasing temperature in the temperature range 223–273 K. The critical strain for the onset of serration decreases with the alloy content. Also, serration on the flow curves becomes more significant for higher alloy content. Fig. 3 indicates the amplitude of the serration as a function of strain for different Ni contents. Both of the results indicate that flow instability is enhanced by the particles.

In addition to flow instability, the tensile properties are also affected. The flow stresses increase while the elongation decreases with alloy content. Fig. 4 gives the plot of flow stress, σ, at 0.2 and 1 % strain versus

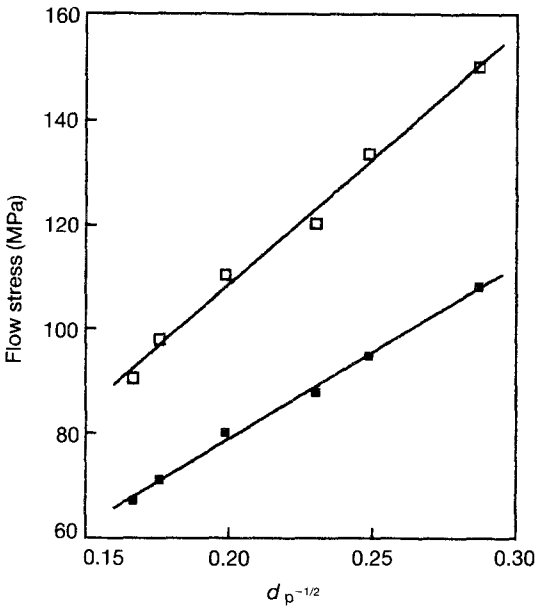

Figure 4 The flow stresses of Al–Mg–Ni alloys at (■) 0.2 and (□) 1% strain as a function of particle spacing at 248 K and $5.7 \times 10^{-4}\ s^{-1}$.

$d_p^{-1/2}$. The flow stress at 0.2 and 1 % strain can be expressed by an equation similar to the Hall–Petch equation, as

$$\sigma = \sigma_o + K d_p^{-1/2} \quad (14)$$

where σ_o is the friction stress and K is the proportional constant. Also, the difference between the 0.2 % flow stress and the 1 % flow stress increases with the value of $d_p^{-1/2}$, indicating that the work-hardening rate is increased. These results show that particles can increase the strength and the work-hardening rate of aluminium alloys.

As the particles are coarse and rigid, they are impenetrable to dislocation and dislocation pile up around the particles is possible. Ashby [8, 9] has also introduced the concept of geometrically necessary dislocations in material containing hard particles. Karlsson *et al.* [25–26] showed that the second phase particles will severely reduce the slip distance, increasing the dislocation density. Then, dislocation multiplication is enhanced by rigid particles among the matrix. As a result, the alloys are strengthened by the particles.

4.3. Apparent activation energies

According to the general expression, Equation 1 or 9, the apparent activation energies, Q, for each alloy can be obtained by measuring the slopes of the plots of ln ε_c versus $1/T$ and ln ε_c versus ln $\dot{\varepsilon}$. The less sensitive term T^{-1} in Equation 9 is dropped. These plots for Al–Mg–Ni and Al–Si alloys are shown in Figs 5–8, respectively. The apparent activation energies and the exponents $\beta(\gamma + 1/2)$ for each alloy are listed in Tables V and VI. The activation energies are about 0.55 eV in Al–Mg–Ni alloys and about 0.35 eV in Al–Si alloys. The activation energies are quite close to that of the Al–Mg binary alloy [3, 13], implying that Mg is responsible for serration in the Al–Mg–Ni

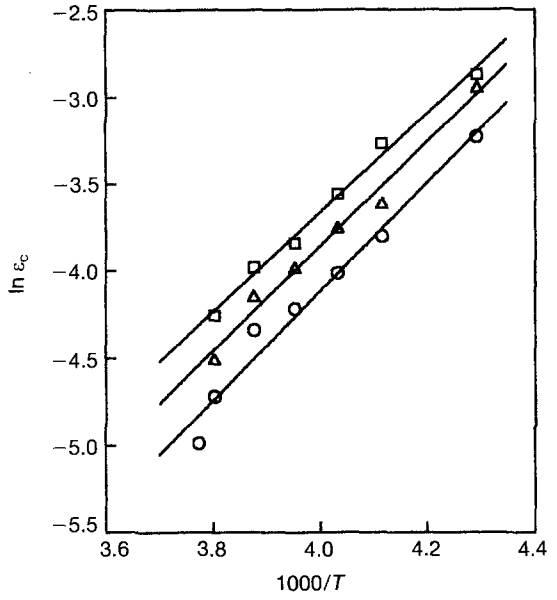

Figure 5 The critical strain of Al–Mg–Ni alloys as a function of temperature at 5.7×10^{-4} s^{-1}: (□) 0.5, (△) 2, (○) 5 wt % Ni, respectively.

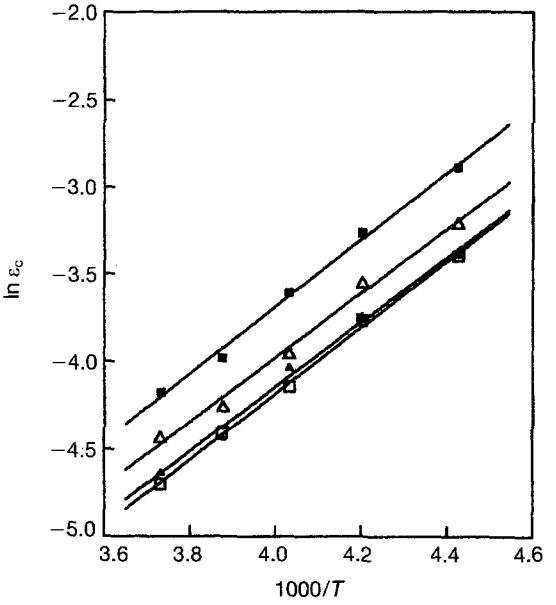

Figure 7 The critical strain of Al–Si alloys as a function of temperature at 5.7×10^{-4} s^{-1}: (■) 1, (△) 4, (▲) 7, (□) 11 wt % Si, respectively.

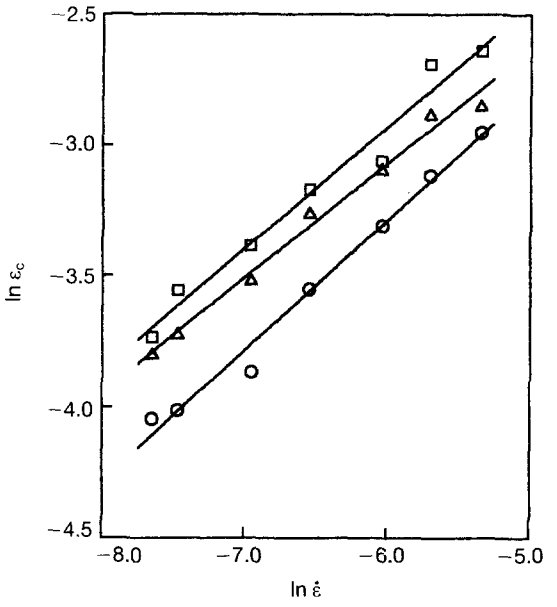

Figure 6 The critical strain of Al–Mg–Ni alloys as a function of strain rate at 248 K: (□) 0.5, (△) 2, (○) 5 wt % Ni, respectively.

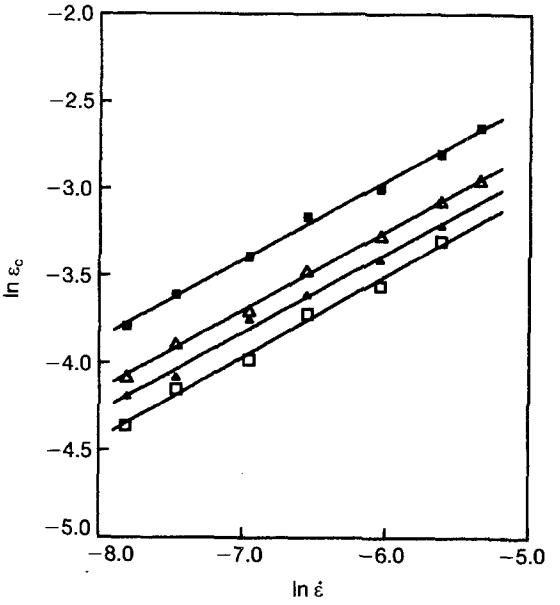

Figure 8 The critical strain of Al–Si alloys as a function of strain rate at 248 K: (■) 1, (△) 4, (▲) 7, (□) 11 wt % Si, respectively.

TABLE V The exponent $\beta(\gamma + 1/2)$ and the apparent activation energies of the Al–Mg–Ni alloys

Alloy (wt % Ni)	$\beta(\gamma + 1/2)$	Q (eV)
0.5	2.18	0.57
1.0	2.21	0.59
2.0	2.24	0.55
3.0	2.10	0.54
4.0	1.92	0.53
5.0	1.99	0.56
6.0	1.83	0.56

system. This result agrees with the fact that the Al–Ni binary alloys do not exhibit flow instability [27]. On the other hand, Si solute in the matrix is responsible for serration in Al–Si alloys [14].

4.4. Effects of particles on the critical strain

Both the critical strain and the amplitude of the serration are dependent on the dislocation density in the matrix [21, 22]. Charnock [23, 24] has accounted for the grain size effect in the PL effect by considering that the dislocation density is inversely proportional to grain size in Equation 12. Chen *et al.* [17, 18] have proved that the grain size dependence of the critical strain can be more properly explained by Equation 13. The dislocation density is increased by decreasing the grain size, d_g, in Equation 12. As mentioned above, the multiplication of dislocation is enhanced by the par-

TABLE VI The exponent $\beta(\gamma + 1/2)$ and the apparent activation energies of the Al–Si alloys

Alloy (wt % Si)	$\beta(\gamma + 1/2)$	Q (eV)
1	2.21	0.37
4	2.19	0.35
7	2.20	0.36
11	2.13	0.35

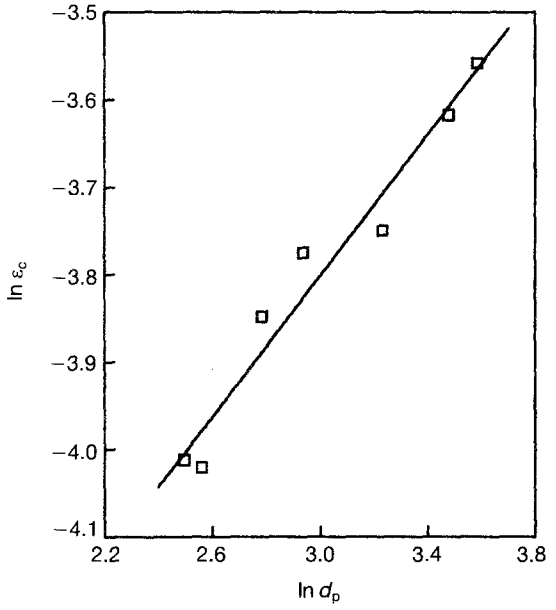

Figure 9 Critical strain as a function of particle spacing for the Al–Mg–Ni alloys at 248 K, $5.7 \times 10^{-4}\ s^{-1}$.

ticles, so that particle spacing should be involved in the expression of dislocation density in Equation 10. Now, a model is put forward, using

$$\rho_m \propto \varepsilon^{\beta}\, d_p^{-n} \tag{15}$$

assuming that the particle effect is dominant and the effect of grain size can be neglected in the present investigation. Listed in Tables III and IV, the variation of grain size is limited in the Al–Mg–Ni alloys, and the particle spacing is less than the grain size. In Al–Si alloys, the grain size is much greater than the particle spacing. As a result, the assumption in Equation 15 is reasonable. Furthermore, Equation 15 is substituted into Equation 6, so that Equation 16 is obtained as follows

$$\dot{\varepsilon} \propto \varepsilon_c^{\beta(\gamma+1/2)}\, d_p^{-n(\gamma+1/2)}\, T^{-1} \exp(-Q/kT) \tag{16}$$

Consequently, the critical strain for the onset of serration should be a function of particle spacing. Equation 16 agrees with the experimental results, that critical strain decreases with decreasing particle spacing. The plot of ln ε_c versus ln d_p at 248 K and strain rate $5.7 \times 10^{-4}\ s^{-1}$, and the plot of ln $\dot{\varepsilon}$ versus ln d_p at 248 K for a given critical strain of 3% for Al–Mg–Ni alloys, are given in Figs 9 and 10, respectively. Similar plots for the Al–Si alloys are given in Figs 11 and 12. Linear fit of the experimental data indicates that Equation 16 is satisfied. Hence, Equation 16 is a proper rationalization of the particle effect.

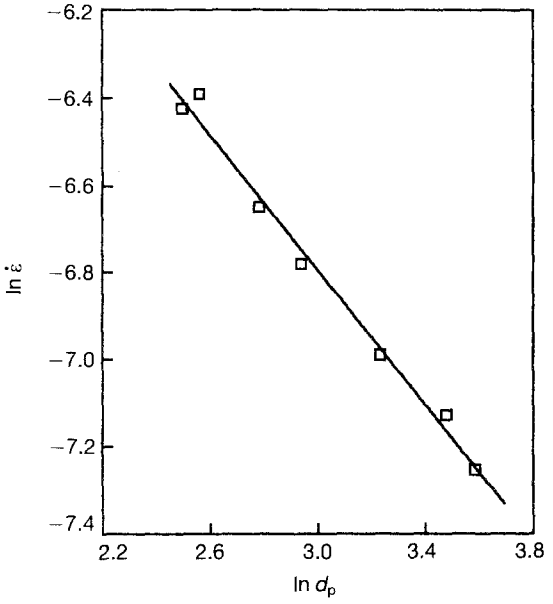

Figure 10 The relationship between strain rate and particle spacing at 248 K for the Al–Mg–Ni alloys when the critical strain is 3%.

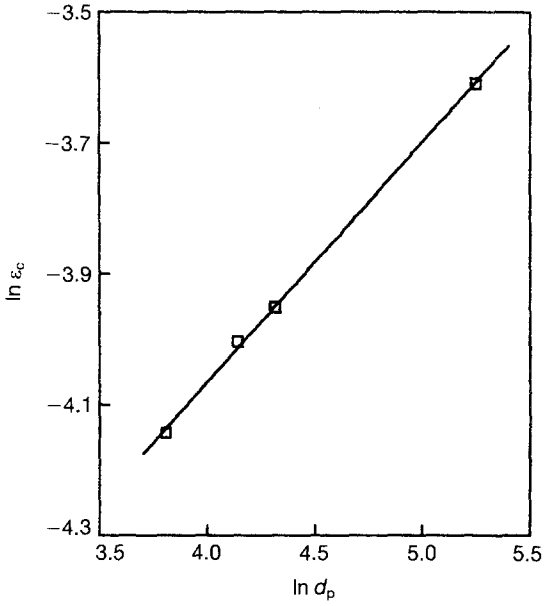

Figure 11 Critical strain as a function of particle spacing for the Al–Si alloys at 248 K, $5.7 \times 10^{-4}\ s^{-1}$.

The slopes of the plots of ln ε_c versus ln d_p, and ln $\dot{\varepsilon}$ versus ln d_p, will give the exponent n/β and $n(\gamma + 1/2)$. The value of exponent n in Equation 15 can be obtained either from n/β or $n(\gamma + 1/2)$ after knowing the values of β and γ. From the slopes of the plots of Al–Mg–Ni and Al–Si alloys, the exponent n/β is 0.42 and 0.36, respectively; while the value of $n(\gamma + 1/2)$ is 0.77 and 0.84, respectively. For most single phase alloys, the value of β is in the range 1.0–1.2, and an average of 1.1 is usually taken [17]. Then, the value of n is about 0.45 and 0.4 for the Al–Mg–Ni and Al–Si alloys, respectively, after multiplying n/β with 1.1. On the other hand, the value of n can be calculated from $n(\gamma + 1/2)$ after knowing the value of $(\gamma + 1/2)$. From the plots of ln ε_c versus $1/T$ in Figs 5 and 7, the value of the exponent $\beta(\gamma + 1/2)$ can

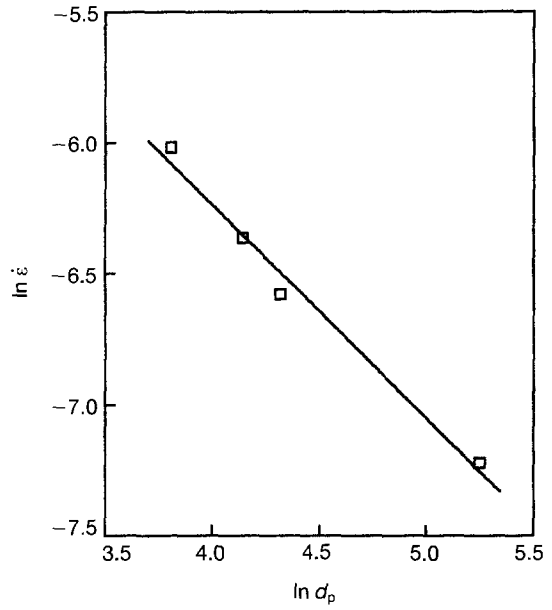

Figure 12 The relationship between strain rate and particle spacing at 248 K for the Al–Si alloys when the critical strain is 3%.

be obtained and is listed in Tables V and VI. As 1.1 is taken for β, so the value of $(\gamma + 1/2)$ is known. In Al–Mg–Ni alloys, the value of $\beta(\gamma + 1/2)$ varies from 1.9 to 2.2, so that the value of n is about 0.39–0.45. In Al–Si alloys, the value is about 2.2, then a value of 0.42 is estimated for n. In the present rationalization, no matter whether the value of n is obtained from n/β or $n(\gamma + 1/2)$, the value of n is in the range 0.4–0.45 for the Al–Mg–Ni and Al–Si alloys. For the rationalization of grain size effect in section 2, the value of n_g is in the range 0.4–0.9 [17]. Hence, both the particles and the grain size have similar effects on the critical strain, assuming that the dislocation density is varied by the particle spacing or the grain size.

5. Conclusions

Al–Mg–Ni and Al–Si alloys contain Al_3Ni and Si particles, respectively, among the matrix. The PL effect of these two alloys is studied in the temperature range 223–273 K and strain rates from 10^{-5} to $10^{-2}\,s^{-1}$. The experimental results can be summarized as follows

1. For both alloys, the critical strain decreases and the amplitude of the serration increases with the alloy content. Hence, serration associated with the PL effect is promoted by the particles.

2. Being independent of the composition, the apparent activation energy is about 0.55 eV for the Al–Mg–Ni alloys and about 0.35 eV for the Al–Si alloys. These results show that the diffusion of Mg and Si is responsible for the flow instability in Al–Mg–Ni and Al–Si alloys, respectively.

3. As the grain size is nearly constant in the Al–Mg–Ni alloys, and is large compared with particle spacing in Al–Si alloys, the decrease in critical strain can be ascribed to the effect of particles. Then, the model proposed by Chen *et al.* is put forward by considering the dislocation density as a function of particle spacing in Equation 15, so that the critical strain can be expressed as a function of particle spacing, as shown in Equation 16.

4. Linear fit of the values ln ε_c versus ln d_p and ln $\dot{\varepsilon}$ versus ln d_p indicates that Equation 16 is appropriate to rationalize the particle effect. The exponent n, showing the dependence of particle spacing on dislocation density, is about 0.4–0.45 for both Al–Mg–Ni and Al–Si alloys.

Acknowledgements

The authors are grateful to Mr J. M. Shyu of National Cheng-Kung University, Taiwan, for joining the experimental work and for useful discussions.

References

1. J. D. BAIRD, in "The Inhomogeneity of Plastic Deformation", edited by R. E. Reed-Hill (American Society for Metals, Metals Park, OH, 1973) p. 191.
2. B. J. BRINDLEY and P. J. WORTHINGTON, *Met. Rev.* **15** (1970) 101.
3. *Idem, Acta Metall.* **17** (1969) 1357.
4. HIROSHI FUJITA and TEIZO TABATA, *ibid.* **25** (1977) 793.
5. P. G. McCORMICK, *ibid.* **19** (1971) 463.
6. J. GUILLOT and J. GRILHE, *ibid.* **20** (1972) 291.
7. P. CETLIN, A. S. GULEC and R. E. REED-HILL, *Met. Trans. A*, **4** (1973) 513.
8. M. F. ASHBY, in "Strengthening Methods in Crystals", edited by A. Kelly and R. B. Nicholson (Elsevier, Amsterdam, 1971) p. 137.
9. *Idem, Phil. Mag.* **19** (1970) 399.
10. M. E. FINE, in "Dispersion Strengthened Aluminium Alloys", edited by Y. W. Kim and W. M. Griffith, (The Minerals, Metals and Materials Society, PA, 1988) p. 116.
11. N. NISHI, S. KAMI, Y. TAKAHASHI, H. KOMOTO and J. G. CONLEY, *ibid.* p. 451.
12. "Metal Handbook", Vol. 8, 8th Edn, (American Society for Metals, Metals Park, OH, 1972) p. 263.
13. SEI MIURA and HIDEAKI YAMAUCHI, *Trans. Jpn. Inst. Met.* **13** (1972) 82.
14. M. NIINOMI, T. KOBAYASHI and K. IKEAD, *J. Mater. Sci. Lett.* **5** (1986) 847.
15. K. MUKHERJEE, C. D'ANTONIO and R. J. MACIAG, *Scripta Metall.* **4** (1970) 209.
16. M. C. CHEN, L. H. CHEN and T. S. LUI, *ibid.* **23** (1989) 655.
17. *Idem, ibid.* **40** (1992) 2433.
18. *Idem, J. Mater. Sci.* **28** (1993) 3329.
19. P. G. McCORMICK, *Acta Metall.* **20** (1972) 351.
20. K. MUKHERJEE, C. D'ANTONIO, R. J. MACIAG and G. FISCHER, *J. Appl. Phy.* **39** (1968) 5434.
21. R. K. HAM and D. JAFFREY, *Phil. Mag.* **15** (1967) 247.
22. A. J. R. SOLER-GOMEZ and W. J. McG. TEGART, *ibid.* **20** (1969) 495.
23. W. CHARNOCK, *ibid.* **18** (1968) 89.
24. *Idem, ibid.* **19** (1969) 209.
25. B. KARLSSON and G. LINDEN, *Mater. Sci. Engng* **17** (1975) 153.
26. *Idem, ibid.* **17** (1975) 206.
27. T. S. LUI, J. D. CHAN and L. H. CHEN, in "Science and Engineering of Light Metals", edited by K. Hirano, H. Oikawa and K. Ikeda (Japanese Institute of Light Metals, Tokyo, 1991) p. 193.

Received 6 September 1993
and accepted 10 May 1994